Convex Optimization for Spring Design in Series Elastic Actuators: From Theory to Practice

Edgar A. Bolívar-Nieto, Gray C. Thomas, Elliott Rouse, and Robert D. Gregg

***Abstract*— Natural dynamics, nonlinear optimization, and, more recently, convex optimization are available methods for stiffness design of energy-efficient series elastic actuators. Natural dynamics and general nonlinear optimization only work for a limited set of load kinetics and kinematics, cannot guarantee convergence to a global optimum, or depend on initial conditions to the numerical solver. Convex programs alleviate these limitations and allow a global solution in polynomial time, which is useful when the space of optimization variables grows (*e.g.*, when designing optimal nonlinear springs or co-designing spring, controller, and reference trajectories). Our previous work introduced the stiffness design of series elastic actuators via convex optimization when the transmission dynamics are negligible, which is an assumption that applies mostly in theory or when the actuator uses a direct or quasi-direct drive. In this work, we extend our analysis to include friction at the transmission. Coulomb friction at the transmission results in a non-convex expression for the energy dissipated as heat, but we illustrate a convex approximation for stiffness design. We experimentally validated our framework using a series elastic actuator with specifications similar to the knee joint of the Open Source Leg, an open-source robotic knee-ankle prosthesis.**

I. Introduction

Series Elastic Actuators (SEA) typically refer to the serial connection between an electric motor, a mechanical transmission, and a spring [1]. The addition of a series spring allows the actuator to regulate torque by controlling the elongation of the spring. Controlling elongation through motor position control is a better-posed problem than controlling torque directly without a spring, especially for systems with a high reduction ratio [2]. As a result, the series spring improves torque tracking at low frequencies compared to highly-geared rigid actuators. However, the series spring reduces torque bandwidth and adds mechanical complexity and mass. In addition to these trade-offs, SEAs can reduce energy consumption by storing and releasing elastic energy [3].

We can categorize the methods to minimize energy consumption via stiffness design into three groups: natural dynamics, nonlinear optimization, and convex optimization. Natural dynamics finds the stiffness of a spring-mass system that would perform the load motion passively. When the load matches the spring-mass system dynamics, the motor will preserve energy by holding its position, *i.e.*, not providing mechanical work. Although this approach provides first-principles intuition to the selection of stiffness, it does not provide useful solutions for arbitrary load motion. Nonlinear optimization can include actuator constraints and arbitrary motion of the load; however, the solution is sensitive to the initial conditions provided to the numerical solver and the solution time is likely prohibitive for real-time computation. These issues become relevant when the space of optimization variables grows (*e.g.*, design of optimal nonlinear springs or co-design of spring, controller, and reference trajectories) or the application benefits from a real-time solution (*e.g.*, variable stiffness actuators).

Solvers for convex optimization can efficiently find a global optimum for programs of moderate size regardless of the initial conditions. Custom solvers for convex quadratic programs with thousands of variables can find a global optimum in a few micro- or milli- seconds [4]. The challenge in convex optimization is identifying that the program is indeed convex [5]. The energy consumption of electric motors, without consideration of the transmission dynamics, is a convex function of the series spring compliance [6]. As a consequence, it is possible to find the global-optimal linear or nonlinear spring that minimizes motor energy consumption for a given task [6]. Convexity is also beneficial to satisfy constraints that may have uncertainty in its definition [7]. This observation made it possible to find optimal values of spring compliance that would satisfy motor speed-torque and spring elongation constraints despite uncertainty in the compliance of the manufactured spring, kinematics and kinetics of the load, and the modeled dynamics [8], [9]. However, all the previous formulations of convexity neglected the dynamics of the transmission, which is a luxury of direct or a few quasi-direct drives [10], [11].

Our contribution

In this paper, we approximate motor energy consumption as a convex function of spring compliance including Coulomb and viscous friction at the transmission (Sec. II-B.2). We provide the first experimental validation that the convex optimization approach of [8], [9] correctly predicts the optimal compliance in real hardware, and moreover in hardware which has notable nonlinear transmission friction effects (Sec. III-C). The type of transmission has a significant impact on its dynamic model [12]. Our framework may not apply if the transmission has significant backlash or if Coulomb and viscous friction do not capture the dynamics of the transmission. The following section will cover the electromechanical and thermal model of an SEA (Sec. II-A) and use this model to formulate the convex approximation of energy in Sec. II-B. Sec. III presents the experimental

This work was supported by the National Science Foundation under Award Numbers 1830360 / 1953908 and 1830338. E. A. Bolívar-Nieto, G. C. Thomas, and R. D. Gregg are with the Electrical Engineering and Computer Science Department; E. Rouse is with the Mechanical Engineering Department; all authors are also with the Robotics Institute at the University of Michigan, Ann Arbor, MI 48109, USA. Email:{ebolivar, rgregg}@ieee.org, {gcthomas, ejrouse}@umich.edu

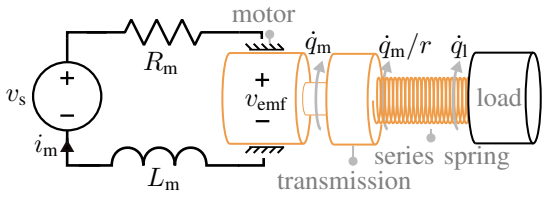

Fig. 1. Electro-mechanical diagram of an SEA. SEA refers to the combination of electric motor, mechanical transmission, and the spring in series with the load. (1), (2) and (4) model the SEA's dynamics.

validation of our framework.

Notation: In this paper, we use $\mathbb{R}_+$ and $\mathbb{R}_{++}$ to denote the set of non-negative and positive real numbers. Column vectors in $\mathbb{R}^n$ are represented by bold lower-case characters. The subindex $\boldsymbol{a}_i$ refers to the i-th element of the vector $\boldsymbol{a}$.

II. Convex Formulation for Series Spring Design

To formulate motor energy consumption and motor speed as convex functions of spring compliance (Sec. II-B.2 and II-B.1), we introduce the background material and dynamics model of SEAs in Sec. II-A. Our expression of energy consumption will assume that the winding temperature does not change considerably during operation. In Sec. III-A, we will use the thermal model in Sec. II-A.2 to assess the impact of winding temperature in our experiments.

A. Modeling of SEAs

In this section, we illustrate the differential and algebraic equations that model the mechanical, electrical, thermal, and elastic behavior of SEAs (Fig. 1). We use these equations to write the motor velocity and energy consumption as convex functions of spring compliance in Sec. II-B.1 and II-B.2, respectively.

1) Electro-mechanical modeling: Using the Newton-Euler method, we balance the torques at the motor side to write the following equations of motion:

$$\tau_\mathrm{m} = I_\mathrm{m}\ddot{q}_\mathrm{m} + b_\mathrm{m}\dot{q}_\mathrm{m} + \mu_\mathrm{t}\mathrm{sign}(\dot{q}_\mathrm{m}) - \frac{\tau_\mathrm{l}}{r}, \tag{1}$$

$$\tau_\mathrm{l} = g(q_\mathrm{l}, \dot{q}_\mathrm{l}, \ddot{q}_\mathrm{l}, \tau_\mathrm{e}), \tag{2}$$

where $I_\mathrm{m} \in \mathbb{R}_{++}$ is the rotor inertia of the motor; $b_\mathrm{m} \in \mathbb{R}_{++}$ the motor and transmission's viscous friction coefficient; $\mu_\mathrm{t} \in \mathbb{R}_{++}$ the torque due to Coulomb friction in the transmission; $r \in \mathbb{R}_{++}$ the reduction ratio of the transmission; $q_\mathrm{m}, \dot{q}_\mathrm{m}, \ddot{q}_\mathrm{m} \in \mathbb{R}$ are the position, velocity, and acceleration of the motor, respectively; $\tau_\mathrm{m}, \tau_\mathrm{l}, \tau_\mathrm{e} \in \mathbb{R}$ are the motor's electromagnetic torque, load torque, and external torque, respectively, *e.g.*, τ_e can represent disturbances or torques from other links in a serial chain; and $g : \mathbb{R}^4 \to \mathbb{R}$ is the function that defines the load dynamics, *e.g.*, in the case of an inertial load with viscous friction the load dynamics are defined by $g = -I_\mathrm{l}\ddot{q}_\mathrm{l} - b_\mathrm{l}\dot{q}_\mathrm{l}$, where I_l is the inertia of the load, and b_l its corresponding viscous friction coefficient. This work assumes that the load trajectory is known and defined by the set of variables $q_\mathrm{l}, \dot{q}_\mathrm{l}, \ddot{q}_\mathrm{l}, \tau_\mathrm{e}$. We model the series spring torque, $\tau_\mathrm{s} = \tau_\mathrm{l}$, as

$$\tau_\mathrm{s} = f(\delta_\mathrm{s}), \tag{3}$$

i.e., mathematically, the spring is a function $f : \mathbb{R} \to \mathbb{R}$ mapping spring elongation, $\delta_\mathrm{s} \coloneqq q_\mathrm{l} - q_\mathrm{m}/r$, to spring torque, τ_s. We assume that $f(\cdot)$ is invertible, *i.e.*, for a given elongation there is a unique torque and vice versa, which is the case for energetically conservative linear or nonlinear springs.

Using Kirchhoff's voltage law across the motor's winding (Fig. 1), we model the electrical behavior of the SEA's motor with the following equation:

$$v_\mathrm{s} = i_\mathrm{m}R_\mathrm{m} + L_\mathrm{m}\frac{di_\mathrm{m}}{dt} + v_\mathrm{emf}, \tag{4}$$

where $v_\mathrm{s} \in \mathbb{R}$ is the voltage of the source, $i_\mathrm{m} \in \mathbb{R}$ is the motor current, $R_\mathrm{m} \in \mathbb{R}_{++}$ is the motor resistance, $L_\mathrm{m} \in \mathbb{R}_{++}$ is the motor inductance, and $v_\mathrm{emf} \in \mathbb{R}$ is the electromotive voltage of the motor. To simplify the analysis, we will assume that the voltage drop across the motor's inductance is negligible compared to the winding resistance voltage, which is a common assumption in practice [12]. Using the equations of electromagnetic torque as a function of current and electromotive voltage as a function of motor velocity (*i.e.*, $\tau_\mathrm{m} = k_\mathrm{t}i_\mathrm{m}$ and $v_\mathrm{emf} = k_\mathrm{t}\dot{q}_\mathrm{m}$, where $k_\mathrm{t} \in \mathbb{R}_{++}$ is the motor torque constant [13]), we rewrite (4) as

$$\tau_\mathrm{m} = v_\mathrm{s}\frac{k_\mathrm{t}}{R_\mathrm{m}} - \dot{q}_\mathrm{m}\frac{k_\mathrm{t}^2}{R_\mathrm{m}}. \tag{5}$$

In this article, we will use the motor constant, $k_\mathrm{m} = k_\mathrm{t}R_\mathrm{m}^{-1/2}$, to calculate heat losses when the motor produces torque. The expressions in (4) and (5) are typical for DC motors and apply to brushless permanent magnet motors using field oriented control, representing the three-phase winding in the quadrature (q-axis) and direct axis with the Clarke and Park transforms [14], [15].

In practice, the rotor inertia, I_m, is the sum of the motor's rotor inertia and the inertia of the transmission (both are available in datasheets or through CAD). However, the motor's viscous friction coefficient, b_m, is rarely documented; one useful approximation is to estimate this coefficient from the no-load current, i_mnl, and no-load speed of the system, $\dot{q}_\mathrm{mnl}$, using the equation: $b_\mathrm{m} = k_\mathrm{t}i_\mathrm{mnl}{\dot{q}_\mathrm{mnl}}^{-1}$. Experimentally, we can identify I_m and b_m fitting a first-order model to a system using i_m as input and $\dot{q}_\mathrm{m}$ as the output [11]. For more details in the experimental identification of the model parameters, we encourage the reader to check [14], [11], [12].

2) Thermal modeling: The electrical diagram in Fig. 2 models the motor winding (T_w) and housing temperatures (T_h) as a function of motor current, as reported in [14], [16], [17]. Balancing heat flux at the T_w and T_h nodes, we write the differential equations that model the thermal behavior as

$$\begin{aligned} P_\mathrm{loss} &= \frac{T_\mathrm{w} - T_\mathrm{h}}{R_\mathrm{wh}} + \frac{d(T_\mathrm{w} - T_\mathrm{a})}{dt}C_\mathrm{wa}, \\ \frac{T_\mathrm{w} - T_\mathrm{h}}{R_\mathrm{wh}} &= \frac{T_\mathrm{h} - T_\mathrm{a}}{R_\mathrm{ha}} + \frac{d(T_\mathrm{h} - T_\mathrm{a})}{dt}C_\mathrm{ha}, \end{aligned} \tag{6}$$

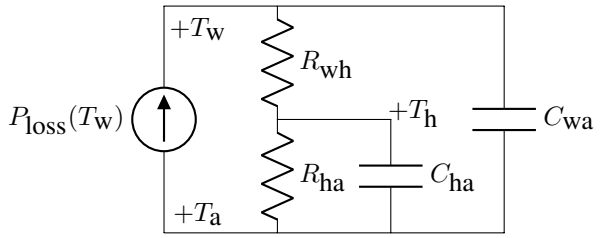

Fig. 2. Thermal model of the motor's winding. It describes winding (T_{w}) and housing (T_{h}) temperatures as a function of the Joule heating generated by the motor current. In this electrical analogy, temperature is equivalent to voltage and heat flux is equivalent to current [14], [16], [17].

where $T_{\mathrm{w}}, T_{\mathrm{h}}, T_{\mathrm{a}} \in \mathbb{R}$ are the winding, housing, and ambient temperatures, respectively; $R_{\mathrm{wh}}, R_{\mathrm{ha}} \in \mathbb{R}_{++}$ are the thermal resistances of winding-to-housing and housing-to-ambient; $C_{\mathrm{wa}}, C_{\mathrm{ha}} \in \mathbb{R}_{++}$ are the thermal capacitances of winding-to-ambient and housing-to-ambient. The power lost due to Joule heating is $P_{\mathrm{loss}} = i_{\mathrm{m}}^2 R_{\mathrm{m}}$. The winding's electrical resistance changes as a function of the winding's temperature based on $R_{\mathrm{m}} = R_{\mathrm{m@a}}(1+\alpha_{\mathrm{Cu}}(T_{\mathrm{w}}-T_{\mathrm{a}}))$, where $R_{\mathrm{m@a}}$ is the winding's electrical resistance at ambient temperature and α_{Cu} is the copper's temperature coefficient of resistance. Some motor manufacturers, such as Maxon Motor, document the thermal capacitances and resistances in the motor's datasheet. If this information is not available, the designer can identify the thermal parameters from temperature measurements in the encapsulation of the winding or housing, as in [14], [16].

B. Convex formulation

An optimization program is convex if the objective and the inequality constraints are convex functions of the optimization variable [5]. In this section, we show how to formulate convex functions to map spring compliance to motor speed (Sec. II-B.1) and motor energy consumption (Sec. II-B.2), even for nonlinear springs (Sec. II-B.3).

1) Minimize any vector norm of motor speed: For a linear spring, the spring torque and elongation relate by the equation $\tau_{\mathrm{s}} = k_{\mathrm{s}}\delta_{\mathrm{s}}$. Using $\tau_{\mathrm{s}} = k_{\mathrm{s}}\delta_{\mathrm{s}}$, the definition of spring elongation, and the fact that $\tau_{\mathrm{s}} = \tau_{\mathrm{l}}$, we write the motor velocity as the following affine function of spring compliance:

$$\dot{q}_{\mathrm{m}}(t) = r(\dot{q}_{\mathrm{l}}(t) - \dot{\tau}_{\mathrm{l}}(t)\alpha_{\mathrm{s}}), \tag{7}$$

where $\alpha_{\mathrm{s}} \in \mathbb{R}_{++}$ denotes the spring compliance. Any norm of $\dot{q}_{\mathrm{m}}$ is a norm of an affine function of α_{s}. Thus, (7) is a convex function of α_{s} [5]. Each norm has a different interpretation, e.g, an ℓ_2, ℓ_∞ -norm will relate to the RMS or peak velocity, respectively. Numerical solvers for convex optimization operate on a vector representation of (7). Thus, we rewrite (7) in vector form, discretizing time in n samples, as $\dot{\boldsymbol{q}}_{\mathrm{m}} = r(\dot{\boldsymbol{q}}_{\mathrm{l}} - \dot{\boldsymbol{\tau}}_{\mathrm{l}}\alpha_{\mathrm{s}})$, where $\dot{\boldsymbol{q}}_{\mathrm{m}}, \dot{\boldsymbol{q}}_{\mathrm{l}}, \dot{\boldsymbol{\tau}}_{\mathrm{l}} \in \mathbb{R}^n$ are the discrete-time versions of motor and load velocity and load torque.

2) Minimize energy consumption: As shown in this section, including Coulomb friction in (1) implies that motor energy consumption is by default a non-convex function of compliance. We will show how to derive a convex approximation of this function to optimize spring compliance. Our derivation will require the following two assumptions: 1) the changes in winding temperature during operation do not modify considerably the motor constant k_{m}, and 2) the initial and final kinematics and kinetics of the load are equal. Many tasks in wearable robotics satisfy our second assumption (*e.g.*, walking, running, cycles of lifting and lowering, *etc*). Using the SEA dynamic model from Sec. II-A, we write the expression of motor energy consumption as

$$\begin{aligned} E_{\mathrm{m}} &= \int_{t_0}^{t_f} i_{\mathrm{m}} v_{\mathrm{s}} dt, \\ &= \int_{t_0}^{t_f} \left(\frac{\tau_{\mathrm{m}}^2}{k_{\mathrm{m}}^2} + \tau_{\mathrm{m}}\dot{q}_{\mathrm{m}} \right) dt, \\ &= \frac{1}{k_{\mathrm{m}}^2} \int_{t_0}^{t_f} \big(\gamma_1^2\alpha_{\mathrm{s}}^2 + 2\gamma_1\gamma_2\alpha_{\mathrm{s}} + \gamma_2^2 + 2b_{\mathrm{m}}\mu_{\mathrm{t}} r|\dot{q}_{\mathrm{l}} - \dot{\tau}_{\mathrm{l}}\alpha_{\mathrm{s}}| \\ &\quad - \frac{\tau_{\mathrm{l}}}{r}\mu_{\mathrm{t}}\mathrm{sign}(\dot{q}_{\mathrm{l}} - \dot{\tau}_{\mathrm{l}}\alpha_{\mathrm{s}}) + \mu_{\mathrm{t}}^2 \mathrm{sign}^2(\dot{q}_{\mathrm{l}} - \dot{\tau}_{\mathrm{l}}\alpha_{\mathrm{s}}) \big) dt + \\ &\quad \int_{t_0}^{t_f} \left(b_{\mathrm{m}}\dot{q}_{\mathrm{m}}^2 + \mu_{\mathrm{t}} r|\dot{q}_{\mathrm{l}} - \dot{\tau}_{\mathrm{l}}\alpha_{\mathrm{s}}| - \tau_{\mathrm{l}}\dot{q}_{\mathrm{l}} \right) dt, \end{aligned} \tag{8}$$

where

$$\gamma_1 = -I_{\mathrm{m}}\ddot{\tau}_{\mathrm{l}} r - b_{\mathrm{m}}\dot{\tau}_{\mathrm{l}} r, \qquad \gamma_2 = I_{\mathrm{m}}\ddot{q}_{\mathrm{l}} r + b_{\mathrm{m}}\dot{q}_{\mathrm{l}} r - \frac{\tau_{\mathrm{l}}}{r}.$$

We can have a convex approximation of (8) by assuming $\mathrm{sign}^2(\dot{q}_{\mathrm{l}} - \dot{\tau}_{\mathrm{l}}\alpha_{\mathrm{s}}) \approx 1$, which holds anytime except when $\dot{q}_{\mathrm{m}} = 0$, and neglecting the term $r^{-1}\tau_{\mathrm{l}}\mu_{\mathrm{t}}\mathrm{sign}(\dot{q}_{\mathrm{l}} - \dot{\tau}_{\mathrm{l}}\alpha_{\mathrm{s}})$, which is accurate when the Coulomb friction or load torque are small. Our approximation applies exclusively to the heat losses at the motor. The mechanical energy provided by the motor, including the mechanical energy dissipated by Coulomb and viscous friction, is a convex function of compliance without any approximation. With those two approximations, we use the Euler method for discrete integration to rewrite (8) as

$$\begin{aligned} E_{\mathrm{m}} \approx \Delta t \sum_{i=1}^{n} \Bigg(&\frac{\boldsymbol{\gamma}_{1i}^2 \boldsymbol{\alpha}_{\mathrm{s}i}^2}{k_{\mathrm{m}}^2} + \frac{2\boldsymbol{\gamma}_{1i}\boldsymbol{\gamma}_{2i}\boldsymbol{\alpha}_{\mathrm{s}i}}{k_{\mathrm{m}}^2} + \frac{\boldsymbol{\gamma}_{2i}^2}{k_{\mathrm{m}}^2} + \frac{\mu_{\mathrm{t}}^2}{k_{\mathrm{m}}^2} - \tau_{\mathrm{l}}\dot{q}_{\mathrm{l}} + \\ &(\mu_{\mathrm{t}} r + \frac{2b_{\mathrm{m}}\mu_{\mathrm{t}} r}{k_{\mathrm{m}}^2})|\dot{\boldsymbol{q}}_{\mathrm{l}i} - \dot{\boldsymbol{\tau}}_{\mathrm{l}i}\boldsymbol{\alpha}_{\mathrm{s}i}| + b_{\mathrm{m}} r^2 (\dot{\boldsymbol{q}}_{\mathrm{l}i} - \dot{\boldsymbol{\tau}}_{\mathrm{l}i}\boldsymbol{\alpha}_{\mathrm{s}i})^2 \Bigg). \end{aligned} \tag{9}$$

The expression (9) is a finite sum of absolute values (ℓ_1 - norm) and quadratic expressions of affine functions of α_{s}; thus, (9) is a convex function of compliance [5]. Notice that the motor energy consumption is a convex-quadratic equation of spring compliance when we neglect the friction at the transmission, reducing to the result in [8].

3) Design of nonlinear series springs: A spring with m piece-wise linear segments approximates a nonlinear spring. With this strategy, we can design nonlinear springs using the compliance vector, $\boldsymbol{\alpha}_{\mathrm{s}} \in \mathbb{R}_{+}^{m}$, as the optimization variable:

$$\begin{aligned} \boldsymbol{\alpha}_{\mathrm{s}i} &= \frac{d\boldsymbol{\delta}_{\mathrm{s}i}}{d\boldsymbol{\tau}_{\mathrm{s}i}}, \\ &= \frac{\dot{\boldsymbol{\delta}}_{\mathrm{s}i}}{\dot{\boldsymbol{\tau}}_{\mathrm{s}i}}, i = 1, \ldots, m. \end{aligned} \tag{10}$$

This definition applies for $\dot{\boldsymbol{\tau}}_{\mathrm{s}i} \neq 0$. For an energetically conservative spring, $\dot{\boldsymbol{\tau}}_{\mathrm{s}i} = 0$ implies that $\dot{\boldsymbol{\delta}}_{\mathrm{s}i} = 0$. Thus, when $\dot{\boldsymbol{\tau}}_{\mathrm{s}i} \neq 0$, $\boldsymbol{\alpha}_{\mathrm{s}i}$ can be $\boldsymbol{\alpha}_{\mathrm{s}i} = \boldsymbol{\alpha}_{\mathrm{s}j}$, where j is the last sample with $\dot{\boldsymbol{\tau}}_{\mathrm{s}j} \neq 0$. The interested reader can follow the procedures in [9] to adapt (9) and (7) for nonlinear springs.

4) Constraining solution to satisfy actuator constraints: The SEA has limitations in torque, velocity, and spring elongation. We can constrain any vector norm of motor velocity using (7) and preserve convexity. Similarly, we can constrain spring elongation using its definition, $\delta_{\mathrm{s}} \coloneqq q_{\mathrm{l}} - q_{\mathrm{m}}/r$. Motor torque is not a convex function of compliance if we include the Coulomb friction at the transmission. A possible solution is to neglect transmission friction, which will preserve convexity [9].

III. Experimental Validation

To experimentally validate the convexity of (9), we measured the energy consumption of an SEA accomplishing a given task with different values of inherent stiffness. We modified the inherent stiffness by stacking 3 to 6 torsional springs in parallel, similar to the Open Source Leg's knee joint, Fig. 3. We controlled the SEA motor and load motor to track the following sinusoidal load position and torque with different values of frequency:

$$\begin{aligned} q_{\mathrm{l}}(t) &= 0.04\sin(2\pi f_{\mathrm{l}} t)\ \mathrm{rad}, \\ \tau_{\mathrm{l}}(t) &= 5\sin(2\pi f_{\mathrm{l}} t)\ \mathrm{N\cdot m}, \end{aligned} \tag{11}$$

where $f_{\mathrm{l}} \in \{1, 2, 4\}$ Hz. Each trajectory satisfied our motor speed-torque and spring elongation ($\delta_{\mathrm{s}} \leq 15$ deg) constraints. Our testbed used permanent magnet brushless motors (U8-KV100, T-motor) distributed as actuator packages (ActPack v0.2b, Dephy Inc), 50:1 planetary transmissions (PL6 Series, Boston Gear), and a rotary torque sensor between the SEA motor and the transmission (TRS600, Futek), Fig. 4. The load motor tracked the reference load position in (11) and the SEA motor controlled the spring elongation to track the reference load torque. Each ActPack reported motor position and q-axis motor current, i_{m}. We calculated the supplied voltage, v_{s}, using (5), i_{m}, and the motor parameters in Table I. We sent reference commands to the motors and logged sensor data at 300 Hz with a Raspberry Pi 3 (Raspberry Pi Foundation). Each ActPack executed position control loops with a 20 kHz PWM. The ActPacks were powered by a Lithium-polymer battery while a benchtop power supply powered the Raspberry Pi 3 and the torque sensor. This paper has a supplemental video of the benchtop apparatus in action.

A. Thermal assumptions

Our convex expression of energy consumption (9) assumes that the load trajectory is periodic and that changes in winding temperature during operation do not modify considerably the motor constant k_{m}. To give some perspective, when the temperature of the winding is close to 100 °C, R_{m} can increase around 30 % (Sec. II-A.2). Increasing R_{m} reduces the motor constant ($k_{\mathrm{m}} = k_{\mathrm{t}}/\sqrt{R_{\mathrm{m}}}$); thus, the motor will dissipate more heat for a given torque. We used the thermal model in (6) to estimate the changes in winding temperature from the experimental values of motor current. The changes in winding temperature were below 2 °C in all our experiments, which are negligible for our calculations of energy consumption. Fig. 5 illustrates the changes in winding temperature for the load trajectory with the highest requirements of motor current.

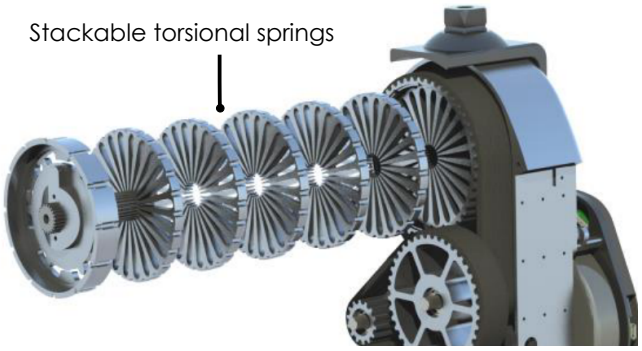

Fig. 3. SEA of the knee joint of the Open Source Leg [16]. The user can stack multiple torsional springs in parallel to change the inherent stiffness of the SEA. Image taken with permission from [18].

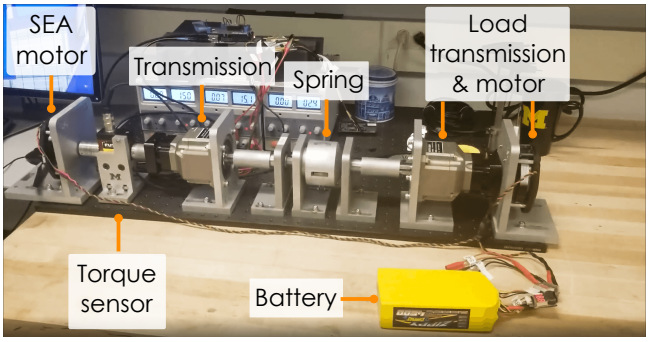

Fig. 4. Instrumented SEA connected to a load actuator. The electric motors, the 50:1 reduction ratio of the transmissions, and the series springs in our experiments match the knee configuration of the Open Source Leg [16].

B. Torque, current, and position for parameter identification

Thanks to the low backlash of the transmission (less than 5 arcmin), we describe its kinematic behavior simply by $q_{\mathrm{ma}} r = q_{\mathrm{m}}$, where q_{ma} is the motor position after the transmission. The kinetic behavior requires consideration of the Coulomb and viscous friction, as mentioned in Sec. II-A. We used the torque from the Futek sensor, τ_{futek}, and the ActPack motor position and corresponding numerical derivatives, $\dot{q}_{\mathrm{m}}$, to estimate the kinetics of the transmission. The torque sensor is in series between the SEA motor and the SEA transmission. Thus, from the third law of motion, the sensor output is equal to

$$\tau_{\mathrm{futek}} = I_{\mathrm{m}}\ddot{q}_{\mathrm{m}} + b_{\mathrm{m}}\dot{q}_{\mathrm{m}} - i_{\mathrm{m}}k_{\mathrm{t}}, \tag{12}$$

$$\tau_{\mathrm{futek}} = \frac{\delta_{\mathrm{s}}k_{\mathrm{s}}}{r} - \mu_{\mathrm{t}}\mathrm{sign}(\dot{q}_{\mathrm{m}}) - b_{\mathrm{mt}}\dot{q}_{\mathrm{m}}, \tag{13}$$

where b_{mt} is the viscous friction coefficient of the transmission. We used least-squares to find the μ_{t} and b_{mt} that minimized $\|\tau_{\mathrm{futek}} - \delta_{\mathrm{s}}k_{\mathrm{s}}r^{-1} + \mu_{\mathrm{t}}\mathrm{sign}(\dot{q}_{\mathrm{m}}) + b_{\mathrm{mt}}\dot{q}_{\mathrm{m}}\|_2$, *i.e.*,

TABLE I

SEA PARAMETERS. WE USED THE MOTOR WINDING RESISTANCE, TORQUE CONSTANT, THERMAL RESISTANCE AND CAPACITANCE EXPERIMENTALLY VALIDATED IN [14]

Parameter	Value
Torque constant*, k_t (N·m/A)	0.14
Terminal resistance*, R_m (mΩ)	279
Continuous torque (N·m)	1.1
Motor inertia, I_m (kg·cm^2)	1.2
Gear ratio, r	50
Viscous fric., b_m (mN·m·s/rad)	3.61
Max. velocity, $\dot{q}_{max}$ (rpm)	2455
Voltage (V)	36
Coulomb friction, μ_t (N·m)	0.036
Thermal resistance winding-housing, R_{wh}, (K/W)	1.1
Thermal resistance housing-ambient, R_{ha} (K/W)	3.5
Thermal capacitance winding-ambient, C_{wa} (W·s/K)	36
Thermal capacitance housing-ambient, C_{ha} (W·s/K)	104

*Values are in the q-axis

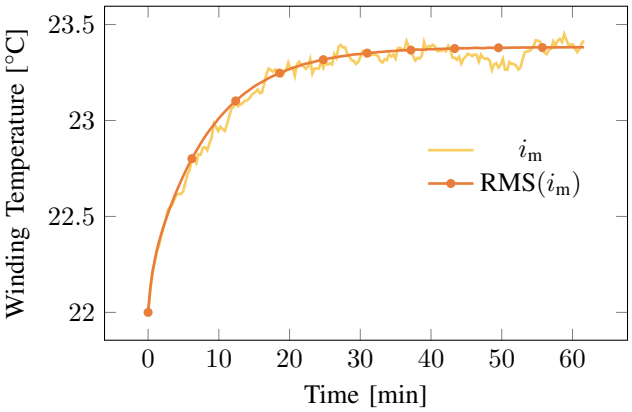

Fig. 5. Estimation of winding temperature for the load trajectory with the highest requirements of motor current. We used the thermal parameters in Table I. i_m is the winding temperature from the measured current readings. The sinusoidal load trajectories (11) lead to sinusoidal motor currents; hence, replacing i_m with its constant RMS value (1.25 A) produced similar results, as shown by the RMS(i_m) line. As a reference, our model (6) converges to a winding temperature of 106 °C after 60 min when changing the RMS current to 8.5 A, which approximates the specifications of the ActPack.

the difference between measured torque and the modeled torque from the spring and transmission. We lumped the transmission and motor viscous friction coefficients to simplify notation. Table I reports the results from the system identification. Fig. 6 illustrates the measured torque, the estimated torque from the motor current, and the output from the transmission model. As a reference, the RMS error between the measured torque and the right hand side of (12) and (13) is 53 and 39 mN·m for the load frequency of 4 Hz and 16 and 10.5 mN·m for the load frequency of 1Hz, respectively. Such accurate models of motor torque are fundamental for calculating energy consumption from (9).

C. Energy as a convex function of compliance

We measured the energy of the motor for each possible value of stiffness when tracking each reference load trajectory in (11). We integrated electrical power, i.e., the product of motor current and supplied voltage, per cycle to estimate the energy consumption of the SEA ActPack and compared it with the energy predicted from our convex approximation

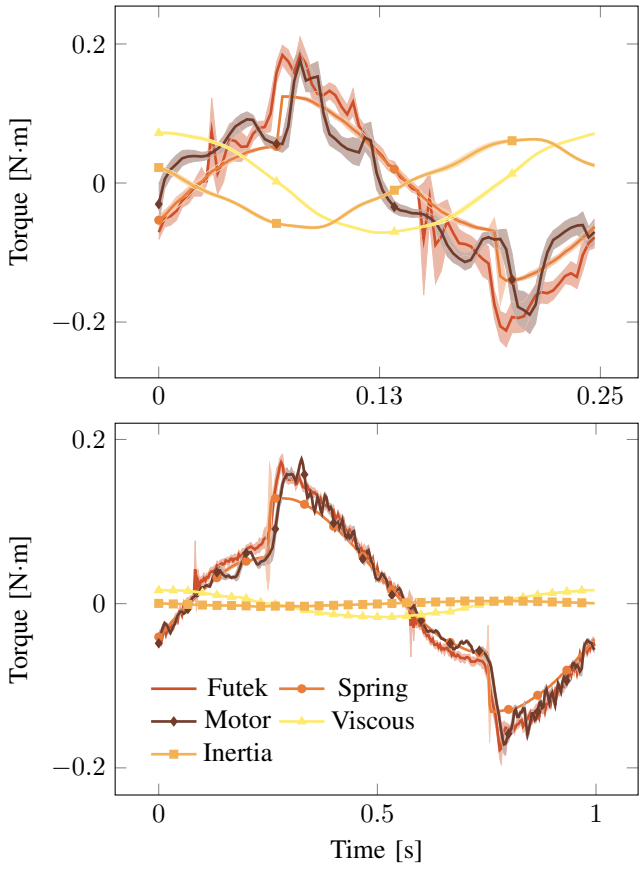

Fig. 6. Measured torque from Futek sensor (Futek), estimated torque from motor current and kinematics (Motor), and estimated torque from spring elongation and transmission dynamics (Spring). (Motor) and (Spring) match the right hand sides of (12) and (13), respectively. The top and bottom figures match the load trajectories with frequencies of 4 and 1 Hz, respectively. As a reference, (Inertia) and (Viscous) lines show the inertia and viscous torques from the motor. Solid lines indicate the mean of our trials. Shaded regions denote two standard deviations from the mean.

in (9), as shown in the violin plots of Fig. 7. The convex approximation of energy in Fig. 7 use the SEA parameters in Table I and measured load torque and position to estimate energy consumption. In addition, we used CVXPY [19] to find the global optimal value of compliance that minimizes (9). For all values of f_l in (11), the optimal value of compliance was 8.1 mrad/(N·m), matching our measurements in Fig. 7.

IV. CONCLUSION

We formulated a convex approximation of SEA energy consumption as a function of spring compliance (9). Our approximation assumes that the kinematics and kinetics of the load are the same at the initial and final time of the task and that changes in temperature winding do not result in significant changes in the electrical winding resistance at room temperature. Motor velocity is an affine function of compliance (7). If there is no complete information on the dynamics of the transmission, designing a series spring that minimizes a vector norm of motor velocity may be beneficial to minimize energy consumption. Our framework assumes that Coulomb and viscous friction represent most of the dynamics of the transmission, which was an accurate

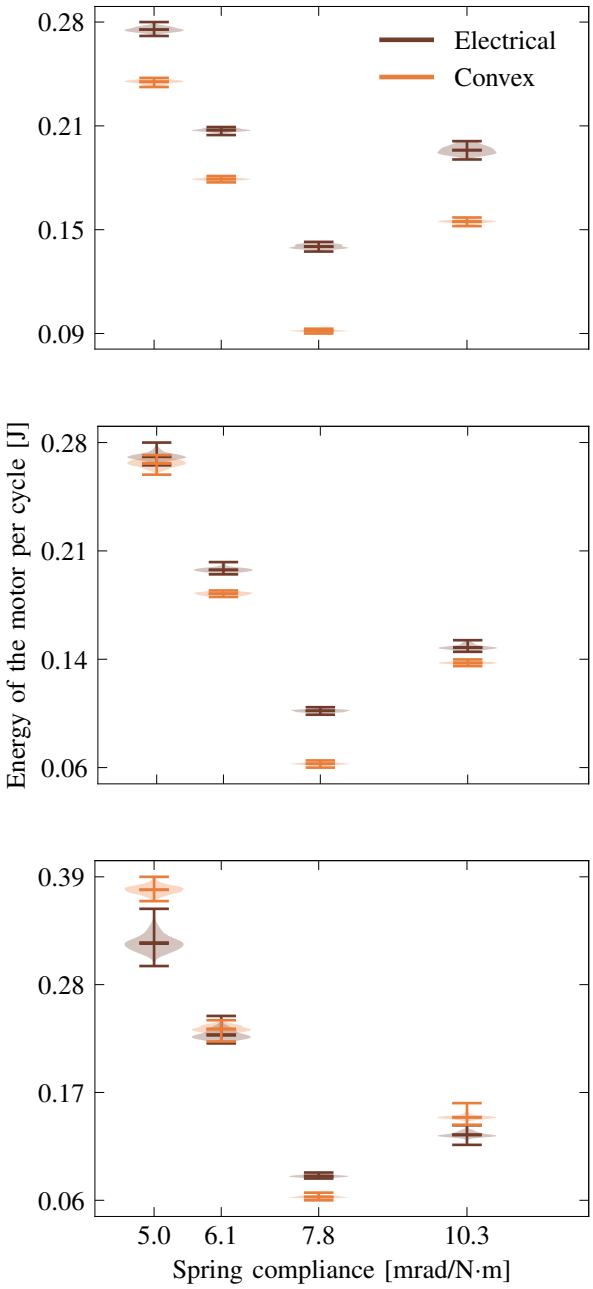

Fig. 7. Energy consumption calculated from the measured motor current and supplied voltage (Electrical) compared to the estimated energy using our convex approximation in (9) (Convex). Our convex approximation used the measured load kinematics and kinetics and the motor parameters in Table I to estimate energy consumption. The values of compliance 5, 6.1, 7.8, and 10.3 mrad/(N·m) correspond to 6, 5, 4, and 3 rotational disc springs connected in series, respectively. The lines on each violin plot represent the minimum, the maximum, and the mean value of energy for each value of compliance. Top, middle, and bottom plots illustrate the energy consumption for 1, 2, 4 Hz load frequency, respectively. As a reference, the global optimal compliance is 8.1 mrad/(N·m) for all frequencies, as predicted by minimizing (9) using CVXPY [19].

estimation for our planetary transmission (Fig. 6). Other kinds of transmissions, such as belts, may need to model the compliance of the transmission itself. The interested reader can extend our framework to account for transmission compliance, which will result in a convex program. However, our framework may not apply if the transmission has significant backlash or if Coulomb and viscous friction do not capture the dynamics of the transmission.

V. Acknowledgments

We thank Ung Hee Lee for the meaningful discussions and his work with system identification of brushless motors.

References

[1] G. Pratt and M. Williamson, "Series Elastic Actuators," in *Proc. 1995 IEEE/RSJ Int. Conf. Intell. Robot. Syst. Hum. Robot Interact. Coop. Robot.*, vol. 1. IEEE Comput. Soc. Press, 1995, pp. 399–406.

[2] D. W. Robinson, "Design and Analysis of Series Elasticity in Closed-loop Actuator Force Control," Ph.D. dissertation, Massachusetts Institute of Technology, 2000.

[3] R. Ham *et al.*, "Compliant actuator designs," *IEEE Robot. Autom. Mag.*, vol. 16, no. 3, pp. 81–94, 2009.

[4] J. Mattingley and S. Boyd, "Automatic code generation for real-time convex optimization," *Convex optimization in signal processing and communications*, pp. 1–41, 2009.

[5] S. P. Boyd and L. Vandenberghe, *Convex Optimization*. New York, NY: Cambridge University Press, 2004.

[6] E. A. Bolívar Nieto, S. Rezazadeh, and R. Gregg, "Minimizing Energy Consumption and Peak Power of Series Elastic Actuators: a Convex Optimization Framework for Elastic Element Design," *IEEE/ASME Trans. Mechatronics*, vol. 24, no. 3, pp. 1334–1345, 2019.

[7] A. Ben-Tal, L. El Ghaoui, and A. Nemirovski, *Robust Optimization*, ser. Princeton Series in Applied Mathematics. Princeton University Press, October 2009.

[8] E. A. Bolívar Nieto, S. Rezazadeh, T. Summers, and R. D. Gregg, "Robust optimal design of energy efficient series elastic actuators: Application to a powered prosthetic ankle," in *IEEE Int. Conf. Rehabil. Robot. (ICORR)*, Aug 2019.

[9] E. Bolívar-Nieto, T. Summers, R. D. Gregg, and S. Rezazadeh, "Series Spring Design for Robust-Feasible Quasi-Direct Drives," *Mechatronics*, under Review.

[10] H. Asada and K. Youcef-Toumi, *Direct-Drive Robots: Theory and Practice*. The MIT Press, 1987.

[11] T. Elery, S. Rezazadeh, C. Nesler, and R. D. Gregg, "Design and Validation of a Powered Knee-Ankle Prosthesis with High-Torque, Low-Impedance Actuators," *IEEE Trans. Robot.*, 2020.

[12] T. Verstraten *et al.*, "Modeling and design of geared DC motors for energy efficiency: Comparison between theory and experiments," *Mechatronics*, vol. 30, pp. 198–213, 2015.

[13] J. M. Hollerbach, I. W. Hunter, and J. Ballantyne, "A Comparative Analysis of Actuator Technologies for Robotics," in *Robot. Rev. 2*, 1992, pp. 299–342.

[14] U. H. Lee, C.-w. Pan, and E. J. Rouse, "Empirical Characterization of a High-performance Exterior-rotor Type Brushless DC Motor and Drive," in *IEEE/RSJ Int. Conf. Intell. Robot. Syst.* IEEE, 2019, pp. 8018–8025.

[15] R. H. Park, "Two-reaction theory of synchronous machines generalized method of analysis-part I," *Trans. Am. Inst. Electr. Eng.*, vol. 48, no. 3, pp. 716–727, jul 1929.

[16] A. F. Azocar, L. M. Mooney, J.-f. Duval, A. M. Simon, L. J. Hargrove, and E. J. Rouse, "Design and clinical implementation of an open-source bionic leg," *Nat. Biomed. Eng.*, vol. 4, no. 10, oct 2020.

[17] T. Lenzi *et al.*, "Design, development, and testing of a lightweight hybrid robotic knee prosthesis," *Int. J. Rob. Res.*, vol. 37, no. 8, pp. 953–976, 2018.

[18] A. F. Azocar, L. M. Mooney, L. J. Hargrove, and E. J. Rouse, "Design and Characterization of an Open-Source Robotic Leg Prosthesis," in *2018 7th IEEE Int. Conf. Biomed. Robot. Biomechatronics*, 2018, pp. 111–118.

[19] S. Diamond and S. Boyd, "CVXPY: A Python-embedded modeling language for convex optimization," *Journal of Machine Learning Research*, vol. 17, no. 83, pp. 1–5, 2016.